

HYDROTHERMAL SYNTHESIS OF ALIGNED HYDROXYAPATITE NANORODS WITH ULTRA-HIGH CRYSTALLINITY

S. Manafi^{1*}, M. R. Rahimipour¹, B. Yazdani¹
S. K. Sadrnezhad^{1,2} and M. H. Amin¹

¹ Materials and Energy Research Center
P.O. Box 31787-316, Karaj, Iran

² Center of Excellence for Production of Advanced Materials
Department of Materials Science and Engineering
Sharif University of Technology, P.O. Box 11365-9466
Tehran, Iran

s-manafi@merc.ac.ir - m-rahimi@merc.ac.ir - bahareh_yd@yahoo.com
sadrnezah@sharif.edu - m-amin@merc.ac.ir

*Corresponding Author

(Received: September 6, 2007 - Accepted in Revised Form: January 30, 2008)

Abstract Hydroxyapatite nanorods aligned with ultrahigh crystallinity and high-yield were successfully synthesized through a hydrothermal approach. In this experiment, a new composition of cetyltrimethylammonium bromide ($(\text{CH}_3(\text{CH}_2)_{15}\text{N}^+(\text{CH}_3)_3\text{Br}^-)$ was designated as CTAP)/ $\text{Ca}(\text{NO}_3)_2/(\text{NH}_4)_2\text{HPO}_4/\text{NaOH}$ and distilled water under hydrothermal condition, to synthesize single crystal HAp nanorods with diameter of 20 ± 10 nm and length of 80 ± 20 nm, was introduced. Crystal phases were determined by X-ray diffraction (XRD). Scanning electron microscope (SEM) was applied to investigate the morphology. The microstructure of the HAp products were further observed by transmission electron microscope (TEM) and high resolution transmission electron microscope (HRTEM) with energy-dispersive X-ray spectroscopy (EDX). The purity and chemical composition of the as-synthesized powder was analyzed by FTIR and inductively coupled plasma atomic emission spectroscopy (ICP).

Keywords Nanorods, Hydroxyapatite, Hydrothermal Synthesis, Crystallinity, Biomaterials and HRTEM

چکیده نانومیله های هیدروکسی آپاتیت منظم با درجه کریستالی بالا با استفاده از روش هیدروترمال با موفقیت سنتز شد. در این کار، یک ترکیب مناسبی از CTAB، نیترات کلسیم، فسفات هیدروژن آمونیم، سود و آب مقطر تحت شرایط هیدروترمال برای سنتز نانومیله های هیدروکسی آپاتیت کریستالی با قطر 20 ± 10 nm و طول 80 ± 20 nm معرفی شدند. فازهای کریستالی توسط دیفرکتومتر (XRD) تعیین شدند. مورفولوژی پودر تولید شده توسط میکروسکوپ الکترونی روبشی (SEM) تعیین شد. آنالیز شیمیایی پودر نهایی و ساختار پودرها توسط میکروسکوپ الکترونی عبوری با قدرت تفکیک بالا (HRTEM) تعیین شد. برای خلوص و ترکیب شیمیایی پودر سنتز شده، از آنالیز های ICP و FTIR استفاده شد.

1. INTRODUCTION

Hydroxyapatite ($\text{Ca}_{10}(\text{PO}_4)_6(\text{OH})_2$, HAp), is the prime constituent of inorganic mineral which is contained in tooth and body tissues. HAp has been used extensively as an artificial bone substitute, in different medical application, due to its biocompatibility, bioactivity, osteoconductivity,

nontoxicity, non-immunogenicity and non-inflammatory behavior [1]. The characteristics of HAp is determined by its morphology, crystallite size, purity, stoichiometry and structure [2-4]. Therefore, many significant synthesis methods have been invented and improved to prepare HAp with controllable properties [4-13]. Especially for nanoscale HAp, there are a lot of especial

behaviours. For example, most HAp materials are implanted in the form of granules and rod [14]; HAp nanophase ceramic has clearly improved the osseointegrative properties [15]; the efficiency of a catalyst supported by nanoscale HAp could also be improved [16]; HAp nanoparticles have an interesting potential as gene and carrier system [17,18]. Nevertheless, due to low reliability, especially in wet environments, the HAp bioceramic cannot be used for heavy load-bearing application, like artificial teeth and bones. Thus, despite their favourable biological properties, the poor mechanical properties of HAp bioceramics have severely hindered their clinical application [19-21]. Therefore, a number of studies have been focused on the improvement of the mechanical properties of HAp bioceramic [22,23] and studies have shown that the mechanical properties of the ceramics could be reinforced remarkably by one dimensional (1-D) nanoscale building blocks, such as nanorod, nanofibers and nanotubes [24-27]. HAp powders can be synthesized by a variety of methods such as solid-state reaction, chemical precipitation and hydrothermal technique [28-30]. Solid-state reactions usually give a stoichiometric and well-crystallized product, but they require relatively high temperatures and long heat-treatment time. Moreover, the sintering ability of such powder is usually low and ultimately results in a lower mechanical properties of the sintered matrixes [30]. In the case of chemical precipitation, nanometer size powders can be prepared. However, their crystallinity and Ca/P ratio, mainly depends on the preparation conditions and in many cases are lower than well-crystallized stoichiometric HAp [30]. The hydrothermal technique usually gives HAp powders a high degree of crystallinity and a Ca/P ratio close to the stoichiometric value [30]. Among the reported studies, however, little work has been done with the preparation of single-crystal hydroxyapatite nanorods. In this work, the hydrothermal technique was developed for the formation of ultra-high crystalline hydroxyapatite nanorods. The nanorods are interestingly crystallized as single crystal with hexagonal heads. These high-quality hydroxyapatite nanorods represent a well-defined nanoscale structure needed for both fundamental studies and clinical applications.

2. EXPERIMENTAL

All the reactants, $\text{Ca}(\text{NO}_3)_2$ (99 % MERCK), $(\text{NH}_4)_2\text{HPO}_4$ (99 % Alfa), and NaOH (96 % Aldrich), were of reagent grade and used without further purification. In a typical experiment, an alkali solution, cetyltrimethylammonium bromide ($((\text{CH}_3(\text{CH}_2)_{15}\text{N}^+(\text{CH}_3)_3\text{Br}^-)$, CTAB)/ $\text{Ca}(\text{NO}_3)_2$ /NaOH/ $(\text{NH}_4)_2\text{HPO}_4$ and distilled water, was selected for this study. As a typical synthesis, two identical solution were prepared by dissolving CTAB (2 g) in 50 ml (0.2 M, 2.36 g) of $\text{Ca}(\text{NO}_3)_2$ and 50 ml (0.12 M, 0.79 g) of $(\text{NH}_4)_2\text{HPO}_4$. The mixing solution was stirred for 30 min until it became transparent. Next, 2 ml of 1 M NaOH aqueous solution and 10 ml of distilled water were added to the solution, respectively. After substantial stirring, the two optically transparent alkali solutions were mixed and stirred for another 30 min. The resulting alkali solution was then transferred into a 30 ml stainless Teflon-lined autoclave and was heated at 150°C for 18 h. The resulting suspension was cooled to room temperature right after the heating and was then stored at a constant temperature of 50°C . After 18 hours, samples were collected and washed several times with distilled and then deionized water. For these experiments, a Siemens D500 powder diffractometer with the $\text{K}\alpha_1$, radiation of copper ($\lambda = 1.5406 \text{ \AA}$), was used and X-ray diffraction patterns were recorded in an angular range of $2\theta = 20\text{-}60^\circ$. The obtained HAp nanorods were characterized with scanning electron microscope, energy-dispersive X-ray spectroscopy (SEM/EDX, XL30). The powder product was further investigated using Fourier transform infrared (FTIR) spectroscopy in a Bruker-IR spectrometer from 500 to 4000 cm^{-1} using the KBr technique and operating in the transmittance mode. The size, distribution and morphology of the samples were analyzed by field emission gun (FEG) transmission electron microscope (TEM), selected area electron diffraction (SAED) observation on a Philips CM200 transmission electron microscope operated at 200 kV. TEM samples were prepared by dispersing the nanorods in ethanol and collecting them on lacey carbon, Cu mesh TEM grids. When HAp damages under the electron beam, small voids are seen within the nanorods giving them a porous appearance [31]. For this reason, all TEM

micrographs were taken, protecting them from even the minimum exposure of electron beam, and no evidence of any electron-beam-induced decomposition damage of the HAp was observed. Finally, the Ca/P impurity ratio of synthesized HAp powders were determined by inductively coupled plasma (ICP) method.

The crystallite size of the powder was evaluated from the peak broadening of XRD patterns based on Scherrer's formula as follows [32]:

$$D = \frac{0.9\lambda}{FWHM \cdot \cos\theta} \quad (1)$$

In which D is the crystallite size (nm), λ is the wavelength of the monochromatic X-ray beam ($\lambda = 0.154\ 056$ nm for CuK α radiation), FWHM is the full width at half-maximum for the diffraction peak under consideration (rad), and θ is the diffraction angle (deg).

3. RESULTS AND DISCUSSION

The XRD patterns in Figure 1 show that the as-synthesized HAp sample at 150°C for 18 h is the hexagonal phase with cell constants $a = 9.22$ Å and $c = 6.885$ Å, which are very close to the values in the literature [33]. It is interesting to know that HAp was obtained at such a low temperature. According to recent research the temperature at which a HAp nanocrystal changes from the amorphous phase to the hexagonal phase when treated with the hydrothermal method was up to 150°C, and a nearly complete hexagonal phase was obtained at 150°C. The shapes of the strong diffraction peaks indicates that the samples are fairly well high crystallized. The crystallinity of HAp powders were synthesized via hydrothermal method which was much higher than those synthesized via normal chemical precipitation [34], sol-gel [35] or normal micromulsion methods [36], and it was attributed to the hydrothermal treatment in the synthetic process [37]. The XRD results showed that the bioceramic were composed of highly crystalline and single phase HAp, and no obvious impurity phase could be found. The shape of the diffraction peaks suggests that the sample could be well crystallized. The broadened nature of

these diffraction peaks implies that, the grain sizes of the samples are of nanometer scale. Estimating from the Debye-Scherrer formula, the average grain size is 20 ± 10 nm.

FTIR analysis revealed the presence of carbon on the surface of the HAp. Figure 2 shows the transmittance of infrared spectrum of synthetic HAp in the 4000-650 cm^{-1} region. A narrow band located near 965 cm^{-1} (962 cm^{-1} in Figure 2) represents the ν_1 mode of PO_4^{3-} ions in apatite. The main signal of phosphate appears in the triply degenerate ν_3 domain (1000-1100 cm^{-1}). The absorption band at 3570 cm^{-1} confirmed the presence of OH groups. The ν_2 peak of CO_3^{2-} is located at 870 cm^{-1} , shows the absorption has resulted from out-of plane stretching. The ν_3 mode, near 1400 cm^{-1} , is the strongest IR peak for

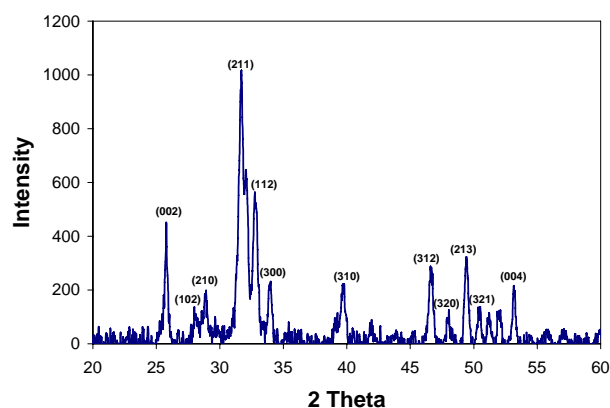


Figure 1. XRD pattern of the as-synthesized HAp nanorods.

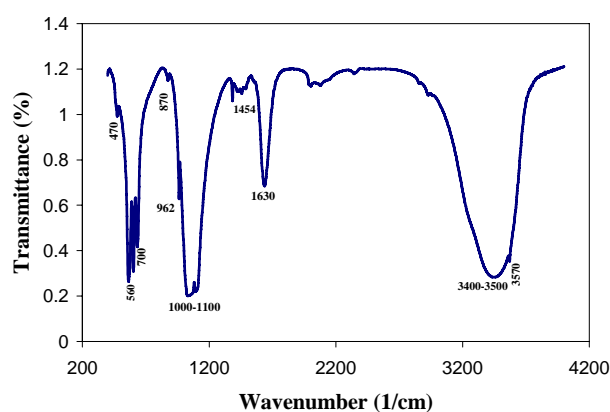
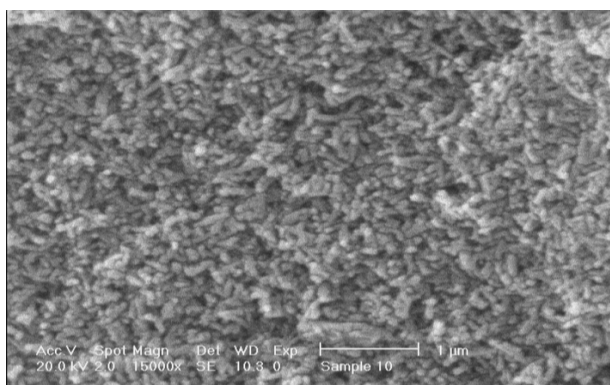


Figure 2. The FTIR spectrum of the HAp nanorods.

carbonate. This peak is actually composed of two bands (1454 and 1421 cm^{-1} , in Figure 2) [38,39]. The shape of the ν_3 signal and the absence of the C-O absorption bands at 700 cm^{-1} indicate that no calcite was associated with the HAp. Carbonate ions can substitute for either OH^- or PO_4^{3-} ions in the apatite structure (type A CO_3^{2-} or type B CO_3^{2-}) [40,41]. The FTIR results, further confirm that the as-synthesized powders are pure HAp.

Figure 3a is the scanning electron microscopic (SEM) image of the as-synthesized HAp obtained at hydrothermal condition, which display nanorods with excellent uniformity. In Figure 3b, the as-synthesized HAp sample shows a typical outstanding morphology, high ordered nanorod structure and high aspect ratio.

A field emission gun (FEG) CM200 high



(a)



(b)

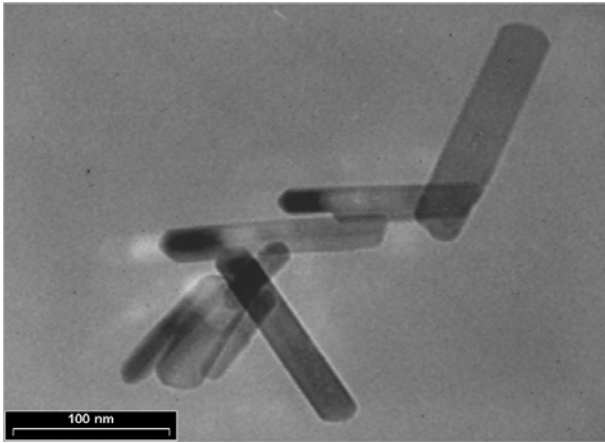
Figure 3. SEM images of (a) as-synthesized HAp obtained at hydrothermal condition and (b) high aspect ratio nanorods.

resolution transmission electron microscope (HRTEM) was used to characterize the HAp nanorods and HAp single crystals, and typical TEM are shown in Figure 4. Figure 4a clearly shows that the product consists of single crystal nanostructures $20 \pm 10\text{ nm}$ in diameter and about $80 \pm 20\text{ }\mu\text{m}$ in length, which are “sub-60 nm HAp nanorods” in this paper. The yield of the prepared nanorod hydroxyapatite estimated by TEM observations is about 99.9 % relative to the samples on copper grids, and the much less contents of the obtained product are nanoparticles (Figure 4b). Thus, the high yield efficiency of this approach for the synthesis of HAp can be concluded, with a ultrahigh crystallinity (Figure 4c) and an excellent yield rather than previous works.

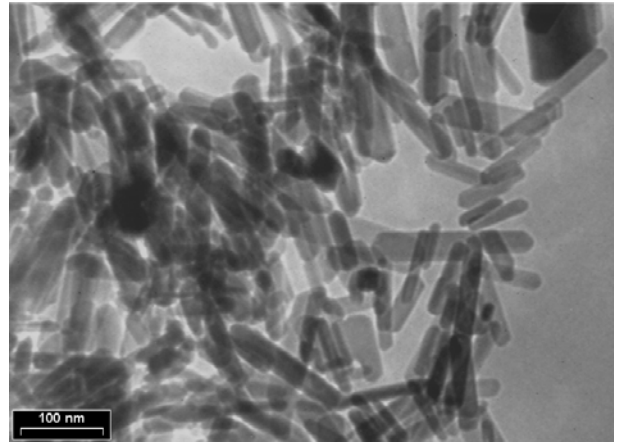
In further investigation, the HAp nanorods were analyzed by HRTEM in detail, and all nanoparticles showed uniform lattice fringes, meaning that no amorphous product was formed. Figure 4d is the HRTEM image of a single crystal HAp nanorod, which clearly indicates that, the HAp nanorod structurally is a uniform single crystalline with ultra-high crystallinity. The interplanar spacing values are calculated from Bragg’s diffraction equation using the diffraction ring diameter and the camera length of the transmission electron microscope. The calculated results indicate the fringe spacing about 0.34 nm observed in Figure 4d agrees with the separation between the 002 lattice planes of hexagonal phase and nanorods which have grown in 001 direction. The EDS spectrum of the nanorod shows that these are only elemental O, Ca and P except the elements of C and Cu, which come from the supported grid for TEM measurement (Figure 4e). The atomic ratio of Ca to P according to EDS semi-quantitative assessment is about 1.67, which was equal to the theoretical value. Those results are in good agreement with the results of ICP.

The histogram in Figure 5a,b indicate that the as-synthesized HA nanorods have diameters of $20 \pm 10\text{ nm}$ and lengths of $80 \pm 20\text{ nm}$, which have suitable aspect ratio from the view point of mechanical properties.

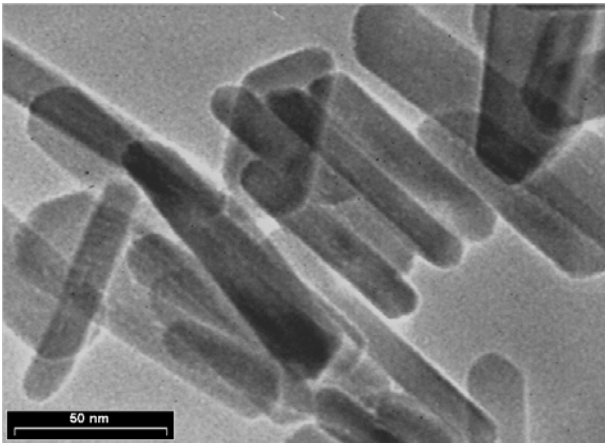
There were some peculiar results in this work which were observed in selected areas of electron diffraction (SAED) pattern. Figure 6 shows the evolution of SAED pattern obtained using a small aperture size in order to ensure the examination of



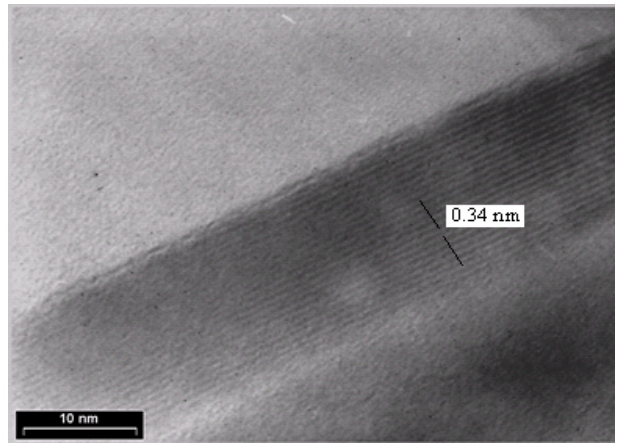
(a)



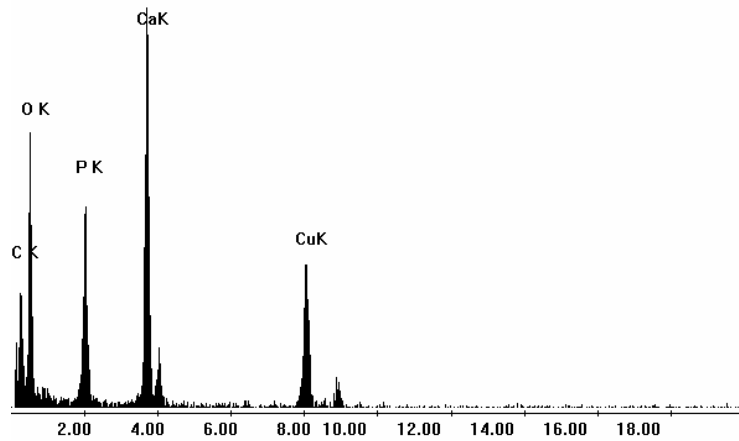
(b)



(c)

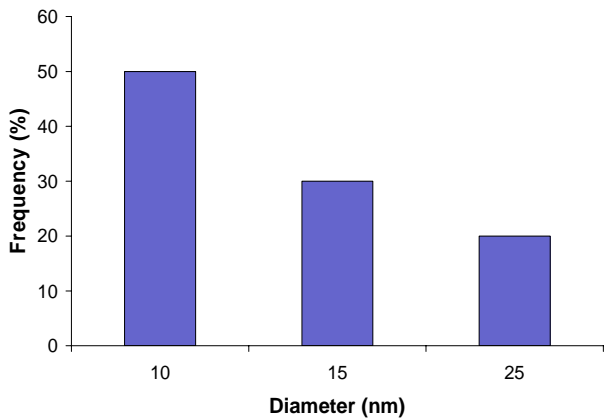


(d)

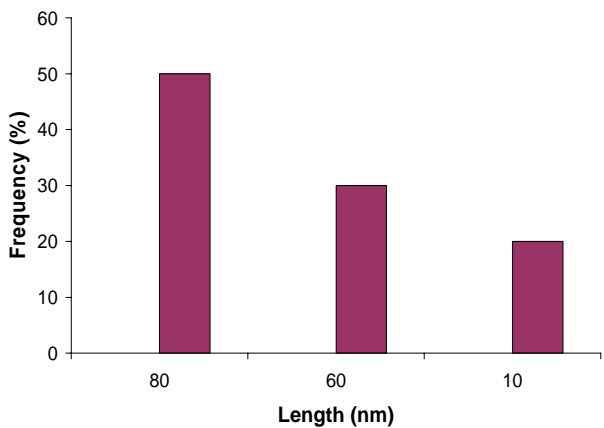


(e)

Figure 4. TEM images of (a) single crystal nanostuctures; (b) high yield efficiency; (c) ultrahigh crystallinity; (d) HRTEM and (e) energy dispersive X-ray analysis (EDAX) of the obtained hydroxyapatite products.



(a)



(b)

Figure 5. (a) Histogram of the nanorod diameter distribution and (b) histogram of the nanorod length distribution.

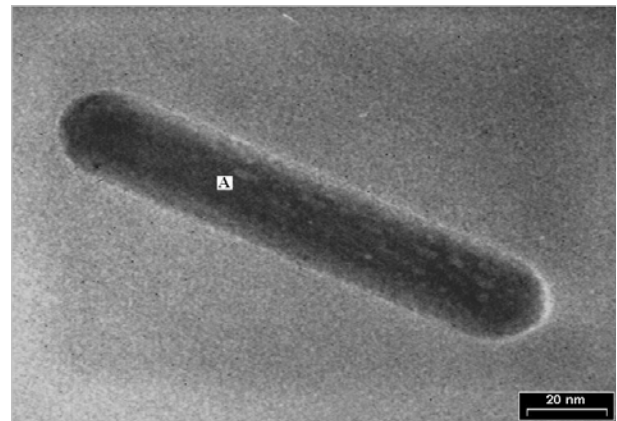
the cross sectional area, belonging to a selected small region of; single crystal and was ca. 0.1 μm in size. This was also done to prevent the contribution of streak and ring distortion of the ED patterns arising from the expected mosaicity of the sample.

SAED observations was performed in the long-axis of the HAp nanorod. The diffraction pattern from area A showed clear spot (Figure 6a) corresponding to an apatite structure with high crystallinity. So, all diffraction patterns from the long-axis of the same nanorod sample showed the same geometry, it was concluded that the apatite fibers preferentially grew along the c-axis to

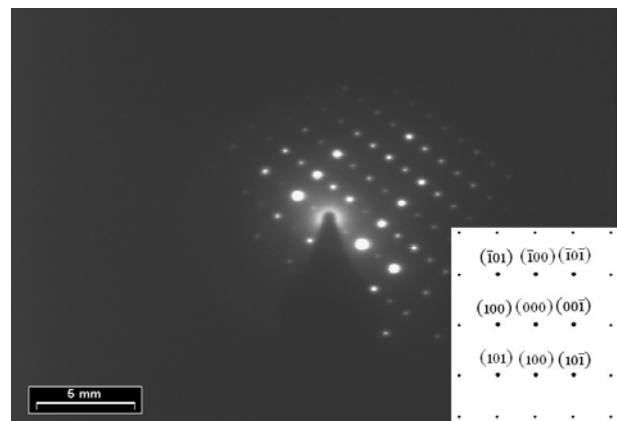
develop the a(b)-plane of hexagonal HAp. The patterns obtained were indexed to the hexagonal lattice of hydroxyapatite viewed along the $\langle 110 \rangle$ zone, and the flat surface is (110) (the lower right insert in Figure 6b).

At the same time, SAED patterns of the samples were consistent with the ultra-high crystallinity, and the diffraction spot could be indexed as the hexagonal phase. This result was in good agreement with the result of XRD.

According to the studies by Xiong, et al [42] and Yao, et al [43], a probable mechanism of formation of HAp might be explained as the following: firstly, the CTAB formed rod-like micelles in which water phase solution containing



(a)



(b)

Figure 6. (a) Individual HAp nanorod (b) A single nanorod selected for undertaking intensive characterization by SAED.

Ca²⁺ or PO₄³⁻ was enwrapped. Because of the concentration difference between the inside (water phase) and outside (oil phase) of the rod-like micelles, the Ca²⁺ or PO₄³⁻ transferred to the surface of the micelles and CTAB-Ca²⁺ or CTAB-PO₄³⁻ rod-like micelles were formed. When the PO₄³⁻ containing solutions were added into the Ca²⁺ contained solutions, HAp clusters were preferentially condensed on the rod-like micellar surface. The micelles acted as nucleating sites for the growth of HAp crystals. During the hydrothermal stage, CTAB-HAp complexes formed and coalesced to form a stable 1-D nanorod structure.

4. CONCLUSION

HAp nanorods with ultra-high crystallinity in the diameter range of 20 ± 10 nm with a high purity have been successfully synthesized by hydrothermal condition. This simple approach should promise us a future large-scale synthesis of this nanostructured material, for many important applications in nanotechnology, for both fundamental/clinical studies in a controlled manner. Our HRTEM observation interestingly illustrated that, the rods are highly stained single crystal with preferred orientation. As a matter of fact, this special structure guarantees its usage in biomaterial world, with outstanding structure.

5. REFERENCES

1. Legeros, R. Z., "Calcium Phosphates in Oral Biology and Medicine", Karger, Basel, Switzerland, (1991).
2. Lazi, S., "Microcrystalline Hydroxyapatite Formation from Alkaline Solutions", *J. Cryst. Growth*, Vol. 147, (1995), 147-154.
3. Suchanek, W. and Yoshimura, M., "Processing and Properties of Hydroxyapatite-Based Biomaterials for Use as Hard Tissue Replacement Implants", *J. Mater. Res.*, Vol. 13, (1998), 94-98.
4. Kumar, R., Prakash, K. H., Cheang, P. and Khor, K. A., "Temperature Driven Morphological Changes of Chemically Precipitated Hydroxyapatite Nanoparticles", *Langmuir*, Vol. 20, (2004), 5196-5200.
5. Gonzalez-Mcquire, R., Chane-Ching, J. Y., Vignaud, E., Lebugle, A. and Mann, S., "Synthesis and Characterization of Amino Acid-Functionalized Hydroxyapatite Nanorods", *J. Mater. Chem.*, Vol. 14, (2004), 2277-2281.
6. Jia, Y., Wiliama, T., Yun, Z. C., Kam, C. T., Jan, M. and Bernard, S., "Hydroxyapatite Nanostructure Material Derived Using Cationic Surfactant as A Template", *J. Mater. Chem.*, Vol. 13, (2003), 3053-3059.
7. Dean-Mo, L., Quanzu, Y., Tom, T. and Wenjea, J. T., "Structural Evolution of Sol-Gel-Derived Hydroxyapatite", *Biomaterials*, Vol. 23, (2002), 1679-1687.
8. Bose, S. and Saha, S. K., "Synthesis and Characterization of Hydroxyapatite Nanopowders by Emulsion Technique", *Chem. Mater.*, Vol. 15, (2000), 4464-4469.
9. Sadasivan, S., Khushalani, D. and Mann, S., "Synthesis of Calcium Phosphate Nanofilaments in Reverse Micelles", *Chem. Mater.*, Vol. 17 (2005), 2765-2770.
10. Wojciech, L. S., Pavel, S., Kullaiiah, B., Richard, E. R., Kevor, S. T. and Victor, F. J., "Mechanochemical-Hydrothermal Synthesis of Carbonated Apatite Powders at Room Temperature", *Biomaterials*, Vol. 23, (2002), 699-710.
11. Han, Y. C., Li, S. P., Wang, X. Y. and Chen, X. M., "Synthesis and Sintering of Nanocrystalline Hydroxyapatite Powders by Citric Acid Sol-Gel Combustion Method", *Mater. Res. Bull.*, Vol. 39, (2004), 25-32.
12. Kim, W. and Saito, F., "Sonochemical Synthesis of Hydroxyapatite from H₃PO₄ Solution with Ca(OH)₂", *Ultrason. Sonochem.*, Vol. 8, (2001), 85-88.
13. Liu, J. B., Li, K. W., Wang, H., Zhu, M. K. and Yan, H., "Rapid Formation of Hydroxyapatite Nanostructures by Microwave Irradiation", *Chem. Phys. Lett.*, Vol. 396, (2004), 429-432.
14. Lin K., Chang, J., Cheng, R. and Ruan, M., "Hydrothermal Microemulsion Synthesis of Stoichiometric Single Crystal Hydroxyapatite Nanorods with Mono-Dispersion and Narrow-Size Distribution", *Mat. Lett.*, Vol. 61, (2007), 1683-1687.
15. Webster, T. J. Ergun, C., Doremus, R. H., Siegel, R. W. and Bizios, R., "Enhanced Osteoclast-Like Cell Functions on Nanophase Ceramics", *Biomaterials*, Vol. 22, (2001), 1327-1333.
16. Kohsuke, M., Takayoshi, H., Tomoo, M., Kohki, E. and Kiyotomi, K., "Hydroxyapatite-Supported Palladium Nanoclusters: A Highly Active Heterogeneous Catalyst for Selective Oxidation of Alcohols by Use of Molecular Oxygen", *J. Am. Chem. Soc.*, Vol. 126, (2004), 10657-10666.
17. Indrajit, R., Susmita, M., Amarnath, M. and Subho, M., "Calcium Phosphate Nanoparticles as Novel Non-Viral Vectors for Targeted Gene Delivery", *Int. J. Pharm.*, Vol. 250, (2003), 25-33.
18. Hartley, T. S., Ben, L. G., Philip, A. W. and Agnes, E. O., "Assembly of Aqueous-Cored Calcium Phosphate Nanoparticles for Drug Delivery", *Chem. Mater.*, Vol. 16, (2004), 4942-4947.
19. Doat, A., Pelle', F., Gardant, N. and Lebugle, A., "Synthesis of Luminescent Bioapatite Nanoparticles for Utilization as a Biological Probe", *J. Solid State Chem.*, Vol. 177, (2004), 1179-1187.

20. Hench, L. L., "Bioceramics: From Concept to Clinic", *J. Am. Ceram. Soc.*, Vol. 74, (1991), 1487-1510.
21. Ducheyne, P., "Material Characteristics Versus in Vivo Behavior", *J. Biomed. Mater. Res.*, Vol. 21, (1987), 219-236.
22. Yaszemski, M. J., Payne, R. G., Hayes, W. C., Lander, R. and Mikos, A. G., "Evolution of Bone Transplantation: Molecular, Cellular and Tissue Strategies to Engineer Human Bone", *Biomaterials*, Vol. 17, (1996), 175-185.
23. Shen, Z., Adolfsson, E., Nygren, M., Gao, L., Kawaoka, H. and Niihara, K., "Dense Hydroxyapatite-Zirconia Ceramic Composites with High Strength for Biological Applications", *Adv. Mater.*, Vol. 13, (2001), 214-216.
24. Suchanek, W., Yashima, M., Kakihana, M., and Yoshimura, M., "Hydroxyapatite/Hydroxyapatite-Whisker Composites without Sintering Additives: Mechanical Properties and Micro Structural Evolution", *J. Am. Ceram. Soc.*, Vol. 80, (1997), 2805-2813.
25. Ramay, H. R. R. and Zhang, M., "Biphasic Calcium Phosphate Nanocomposite Porous Scaffolds for Load-Bearing Bone Tissue Engineering", *Biomaterials*, Vol. 25, (2004), 5171-5180.
26. Yang, W., Araki, H., Kohyama, A., Thaveethavorn, S., Suzuki, H. and T. Noda, "Fabrication in-Situ Sic Nanowires/Sic Matrix Composite by Chemical Vapour Infiltration Process", *Mater. Lett.*, Vol. 58, (2004), 3145-3148.
27. Kobayashi, S. and Kawai, W., "Development of Carbon Nanofiber Reinforced Hydroxyapatite with Enhanced Mechanical Properties", *Composites: Part A*, Vol. 38, (2007), 114-123.
28. Elliott, J. C., "Structure and Chemistry of the Apatites and other Calcium Orthophosphates", Elsevier, Amsterdam, Netherlands, (1994).
29. Narasaraju, T. S. B. and Phebe, D. E., "Some Physico-Chemical Aspects of Hydroxyapatite", *J. Mater. Sci.*, Vol. 31, (1996), 1-21.
30. Byrappa, K., "Handbook of Hydrothermal Technology", Noyes Publications/William Andrew Publishing, LLC, U.S.A., (2001).
31. Landi, S. E., Tampieri, A., Celotti, G. and Sprio, S., "Densification Behaviour and Mechanisms of Synthetic Hydroxyapatites", *J. Eur. Ceram. Soc.*, Vol. 20, (2000), 2377-2387.
32. Jenkins, R. and Snyder, R. L., "Introduction to X-Ray Powder Diffraction", John Wiley and Sons, New York, U.S.A., (1996).
33. Komlev, V. S., Barinov, S. M. and Koplík, E. V., "A Method to Fabricate Porous Spherical Hydroxyapatite Granules Intended for Time-Controlled Drug Release", *Biomaterials*, Vol. 23, (2002), 3449-3454.
34. Engin, N. O. and Tas, A. C., "Manufacture of Macroporous Calcium Hydroxyapatite Bioceramics", *J. Eur. Ceram. Soc.*, Vol. 19, (1999), 2569-2572.
35. Kuriakose, T. A., Kalkura, S. N., Palanichamy, M., Arivuoli, D., Dierks, K., Bocelli, G. and Betzel, C., "Synthesis of Stoichiometric Nano Crystalline Hydroxyapatite by Ethanol-Based Sol-Gel Technique at Low Temperature", *J. Cryst. Growth*, Vol. 263, (2004), 517-523.
36. Lim, G. K., Wang, J., Ng, S. C. and Gan, L. M., "Processing of Fine Hydroxyapatite Powders Via an Inverse Micro Emulsion Route", *Mater. Lett.*, Vol. 28, (1996), 431-436.
37. Byrappa, K., "Handbook of Hydrothermal Technology", Noyes Publications/William Andrew Publishing, LLC, U.S.A., (2001).
38. Doi, Y., Moriwaki, Y., Aoba, T., Takahashi, J. and Joshin, K., "ESR and IR Studies of Carbonate-Containing Hydroxyapatites", *Calcif. Tissue Int.*, Vol. 34, (1982), 178-181.
39. Reigner, P., Lasaga, A. C., Berner, R. A., Han, O. H. and Zilm, K. W., "Mechanism of CO (Super 2-) 3 Substitution in Carbonate-Fluorapatite; Evidence From FTIR Spectroscopy", *Am. Mineral.*, Vol. 79, (1994), 809-818.
40. Elliot, J. C., "PhD Thesis, University of London", London, England, (1964).
41. Bonel, G. A., "Contribution an L'etude De La Carbonation Des. Apatites", *Ann. Chim.*, Vol. 7, (1972), 65-87.
42. Xiong, Y. J., Xie, Y., Yang, J., Zhong, R., Wu, C. Z. and Du, G. A., "In Situ Micelle-Template-Interface Reaction Route to Cds Nanotubes and Nanowires", *J. Mater. Chem.*, Vol. 12, (2002), 3712-3718.
43. Yao, J., Tjandra, W., Chen, Y. Z., Tam, K. C., Ma, J. and Soh, V., "Hydroxyapatite Nanostructure Material Derived Using Cationic Surfactant as a Template", *J. Mater. Chem.*, Vol. 13, (2003), 3053-3057.